Academic Journal of Science and Technology
ISSN: 2771-3032 | Vol. 15, No. 1, 2025

Thin Plate Damage Analysis Based on Transient Displacement Response

Chen Hu, Ke Ding

Central South University of Forestry and Technology, Changsha 410004, China

Abstract: This study systematically simulates and analyzes the dynamic response of a thin plate structure under different damage conditions based on a transient model, aiming to evaluate the performance of Wave Atom transform, wavelet packet transform, and Curvelet transform in damage detection. By applying random initial displacement excitations to the thin plate structure and using optimized load step settings, the impact of different damage severities, damage ranges, boundary damage, and damage spacing on the dynamic response of the structure is analyzed. The results show that both Wave Atom and Curvelet transforms can effectively identify the precise location of large damages, especially performing well in high-frequency responses, but their ability to detect minor damages is weaker. The wavelet packet transform exhibits excellent localization accuracy, especially for minor damages, but due to its limited spatial localization ability, it is prone to misinterpreting high-frequency components of external excitations as damage features, leading to an "over-interpretation" phenomenon. Overall, the Wave Atom transform performs best at high damage levels, Curvelet transform shows strong detection capability in boundary damages and large damage ranges, while the wavelet packet transform has an advantage in locating minor damages. This study provides reliable data support and a theoretical basis for damage detection and serves as a reference for structural integrity analysis.

Keywords: Thin plates; Wave Atom transform; Wavelet packet transform; Curvelet transform; damage.

1. Introduction

In the vast field of modern engineering, the application of thin plate structures has permeated several key industries, including aerospace, aviation, and the automotive sector. These industries place stringent demands on the safety and stability of thin plate structures, making them a focal point of attention for both the public and professionals. However, complex environmental factors such as fatigue, corrosion, and overloads can lead to various forms of damage, such as cracks and fractures, in thin plate structures. These damages directly affect the performance and quality of the plates and may further pose a threat to the safety and stability of the entire engineering project. Therefore, identifying and assessing the degree of damage in thin plate structures is crucial to ensuring engineering safety.

The field of structural damage diagnosis originated from fault detection in mechanical equipment, with its early developments dating back to the early 1960s. The increasing demand for high precision in the performance and structural reliability of aerospace and military equipment spurred the formation and evolution of structural damage diagnosis concepts. In this context, both the theoretical and practical aspects of fault diagnosis in mechanical equipment gained widespread attention and research. Over time, this field has gradually expanded its scope, encompassing a wide range of industries and sectors, including aerospace, civil engineering, and transportation, among others.

M.J. Manjoine classified damage into three stages: the development of continuous slippage, the initiation of permanent damage, and the propagation of permanent damage until failure. In most cases, structural damage can be viewed as a micro-change in stiffness, akin to the development of cracks. In this context, the damage discussed in this study can be understood as the expansion of such "cracks" to a certain extent, leading to noticeable changes in stiffness that affect vibration modes, natural frequencies, vibration acceleration, strain responses, and other structural characteristics. From this perspective, damage identification can be divided into four progressive stages: Detection, which determines whether damage exists in the structure; Localization, which identifies the exact geometric location of the damage; Assessment, which quantifies the severity of the damage; and Prediction, which estimates the remaining useful life of the structure.

In recent years, numerous researchers have introduced various innovative methods for structural damage detection. For instance, Sining Huang et al. [3] proposed a new damage detection technique based on sparse regularization models and a random extended Kaczmarz iterative (REK) algorithm. This method addressed the ill-conditioning problem in damage identification and improved computational efficiency by employing different threshold operators and iterative techniques, including conventional, partial, and rapid maximum distance extended Kaczmarz iteration. The method proved to be highly effective in quickly locating damage, accurately identifying its severity, and offering strong robustness in noisy environments. Similarly, Liu W et al. [4] developed a system based on convolutional neural networks (CNN) to detect structural damage in railroad switches. The system used ultrasonic guided wave signals, processed through multi-layer convolutional networks to extract deep features and classify the data. This approach demonstrated an accuracy rate exceeding 91%, outperforming traditional damage detection methods and showing strong generalization capabilities for real-world railroad switch damage detection tasks. Makiabadi H M et al. [5] presented a method for damage localization and severity assessment using static deformation measurements induced by moving loads, combined with model updating techniques. The "Deformation Influence Line Indicator" (DILI) was proposed as the objective function, and a hybrid algorithm (HESOS-SA) combining Enhanced Symbiotic Organisms Search (ESOS) and Simulated Annealing (SA) algorithms was introduced.

The results showed that the HESOS-SA algorithm effectively identified damage, even in the presence of noise.Yuan P P et al. [6] proposed a novel damage detection and localization method based on Variational Mode Decomposition (VMD) and Chirplet Transform (CT), simulating real environmental conditions such as regular and irregular wave loads and wind loads. The method analyzed changes in time-frequency energy before and after damage, achieving accurate damage localization and quantitative analysis, with validation under various operational conditions. The findings demonstrated that the VMD and CT-based approach was effective for detecting and quantifying damage in frame structures.Yang Haijun et al. [7] proposed a two-stage structural damage detection method based on an improved modal strain energy index and a DBO-BP neural network. The method used an enhanced normalized modal strain energy damage index for localization analysis and optimized the BP neural network using a modified beetle optimization algorithm (DBO). Experimental validation on concrete plate and planar rigid frame structures demonstrated the method's effectiveness, with an error rate of just 0.4%.Barbosh M et al. [8] introduced a damage visualization method using Acoustic Emission (AE) technology combined with Wavelet Packet Transform (WPT) for signal decomposition and Gaussian Mixture Models (GMM) for classification. This approach efficiently visualized damage location during various loading stages, with concrete beam experiments showing its effectiveness in early-stage damage detection.Yao Xiaojun et al. [9] proposed a mutation-based damage identification method combining VMD and Autoregressive Integrated Moving Average (ARIMA) models. The method utilized power spectra to determine the initial frequency and number of modes to be decomposed. It decomposed non-stationary vibration signals using VMD and fitted each signal component with ARIMA, followed by damage localization based on frequency and mode shapes. The approach showed promising results in both stationary and non-stationary excitations. Yanfang H et al. [10] developed a damage localization method based on the rate of change of autocorrelation peak values from random vibration responses. By calculating the autocorrelation functions of measured points and identifying peak values, this method successfully localized damage based on the largest changes in adjacent measurement points' autocorrelation peaks. The method demonstrated high sensitivity to damage and strong noise resistance. Moharana S [11] used a continuous shear lag model to evaluate damage detection by constructing a 3D finite element model for effective point-driven impedance. The method showed superior efficiency and accuracy for damage detection compared to impedance-based models, with excellent experimental results.Lu Y et al. [12] proposed an unsupervised structural damage detection, localization, and quantification method based on Bidirectional Long Short-Term Memory (BiLSTM) networks and Generalized Extreme Value Distribution (GEVD) models. This method reconstructed sensor response data using the BiLSTM network, using reconstruction errors as damage-sensitive features for detection and localization. Validation with numerical models and real data from cable-stayed bridges demonstrated the method's robustness in detecting and quantifying damage under limited sensor configurations.Yu Qiang et al. [13] developed the E-DenseNet model, which combines Empirical Mode Decomposition (EMD) and Dense Convolutional Neural Networks (DenseNet) for structural damage identification. This model decomposed acceleration signals into intrinsic mode functions (IMFs) using EMD and used DenseNet for signal reconstruction and damage identification. The method showed superior accuracy in damage identification compared to other models like ResNet and CNN.Feng Zike et al. [14] integrated Deep Belief Networks (DBN) and Long Short-Term Memory (LSTM) networks through a hybrid learning mechanism to extract high-level abstract features and capture data sequence correlations. The method was effective in reducing redundancy and extracting sensitive damage features, with experimental validation showing its applicability in detecting multiple damage scenarios.Yilmaz Z et al. [15] conducted a numerical analysis of a four-layer reinforced concrete building model to evaluate damage detection using modal participation ratios. The study assessed both single-layer and cumulative damage scenarios, demonstrating that changes in modal participation ratios are highly sensitive to damage and can be used to detect damage location, severity, and progression.

2. Establishment of Thin Plate Models

The finite element analysis software is employed to model and analyze a square thin plate structure. The thin plate is designed as a square with planar dimensions of 1.275 m × 1.275 m, and a thickness of 0.01 m. The material properties are based on typical metallic material parameters: Young's modulus of 192 GPa, Poisson's ratio of 0.25, and a material density of 7800 kg/m³.

To ensure a balance between computational accuracy and efficiency, a grid-based meshing scheme is adopted for the thin plate model. The model is divided into a uniform quadrilateral mesh within the plane, with a cell size of 0.005 m × 0.005 m. In both the length and width directions, 255 elements are used, forming a 256 × 256 node distribution. This meshing strategy ensures adequate computational accuracy while avoiding excessive consumption of computational resources.

Random initial displacements were applied to the finite elements under static conditions to systematically simulate and analyze the dynamic response. The approach first precisely applies a randomly distributed initial displacement excitation to the thin plate structure and then activates a time integration algorithm to capture the structural dynamic evolution. The transient model sets the initial displacement in the Z-direction for element 51128 to 0.01 meters to simulate transient forces. The time window is controlled within the 0 to 0.5-second range, capturing the complete transient response characteristics of the thin plate under damage conditions.

When the thin plate structure is subjected to external excitation, it produces a complex transient dynamic response, including the superposition of multi-modal elastic waves. The damaged region acts as a scattering source for wave propagation, altering the original wave field distribution and giving rise to phenomena such as scattered waves, mode conversion, and local resonance.

To ensure the effectiveness and computational efficiency of the analysis, the simulation process adopts an optimized load step setting, with the main load step set to 3 and subdivided into 11 sub-load steps within each main load step, creating a multi-scale computational framework. Among all the generated time-series data, the study focuses on the Z-direction displacement field data, as displacements in this direction exhibit the highest sensitivity and distinguishability

for thin plate damage characterization. This enables the comprehensive capture of key features such as local vibration anomalies in the thin plate structure under damage influence, providing reliable data support and a theoretical foundation for subsequent damage localization, severity assessment, and structural integrity analysis. Fig.1 below illustrates the transient model with initial displacement.

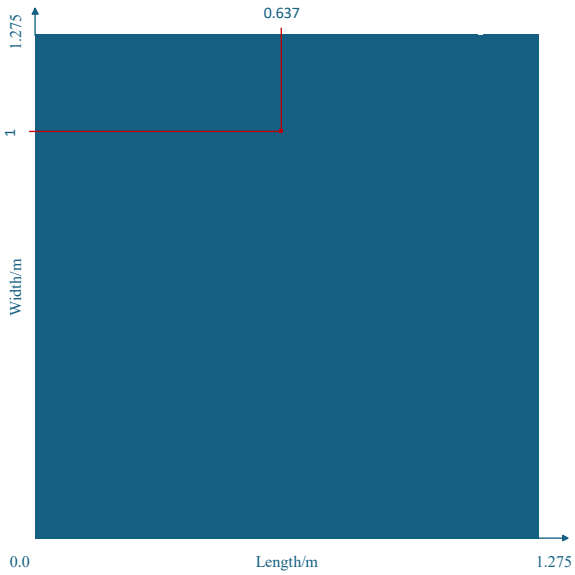

Figure 1. Transient model with initial displacement

3. Derivation of Theoretical Solutions

3.1. Wavelet Packet Analysis

Wavelet packet analysis (WPA) is an extension and generalization of the Continuous Wavelet Transform (CWT) and Discrete Wavelet Transform (DWT). Unlike standard wavelet analysis, which only subdivides the low-frequency part, wavelet packet analysis recursively decomposes both the high-frequency and low-frequency parts of the signal, thus providing a more flexible and refined multi-resolution analysis framework. Wavelet packet analysis extends the orthogonal basis generation mechanism in traditional multi-resolution analysis (MRA) to construct a function library with adaptive band allocation ability. Let the scale function $\phi(t)$ and the parent $\psi(t)$ wavelet satisfy the two-scale equation:

$$\phi(t)=\sqrt{2}\sum_{k\in\mathbb{Z}}h_k\phi(2t-k),\quad \psi(t)=\sqrt{2}\sum_{k\in\mathbb{Z}}g_k\phi(2t-k) \tag{1}$$

h_k and g_k are the coefficients of the low-pass and high-pass filters, respectively, which satisfy the orthogonal condition.

$$\sum_k h_k h_{k-2n}=\delta_{n,0}, g_k=(-1)^k h_{1-k} \tag{2}$$

Family of wavelet packet functions is defined recursively $\{W_n(t)\}_{n\in\mathbb{N}}$

$$\begin{cases} W_{2n}(t)=\sqrt{2}\sum_k h_k W_n(2t-k) \\ W_{2n+1}(t)=\sqrt{2}\sum_k g_k W_n(2t-k) \end{cases} \tag{3}$$

The initial condition is $W_0(t)=\phi(t), W_1(t)=\psi(t)$,so as to generate a complete time-frequency atomic library.

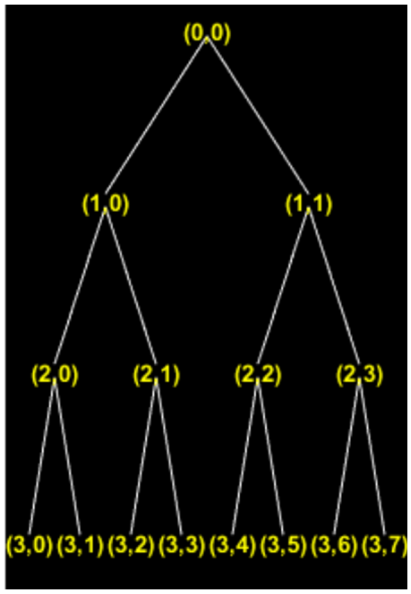

Figure 2. Wavelet packet decomposition tree diagram

Wavelet packet decomposition provides a redundant dictionary of signal representations, and in order to obtain the optimal signal representation, the best basis needs to be selected in the complete binary tree. Let the information cost function E(·) satisfy the additiveness:

$$E(s)=\sum_i E(s_i) \tag{4}$$

s is the signal, s_i is its component. Commonly used information cost functions include:

Shannon Entropy:

$$E_1(s)=-\sum_i |s_i|^2 \log|s_i|^2 \tag{5}$$

Concentration Entropy:

$$E_1(s)=-\sum_i |s_i|^2 \log|s_i|^2 \tag{6}$$

l^p norm:

$$E_3(s)=(\sum_i |s_i|^p)^{1/p}, p\geq 1 \tag{7}$$

For a complete wavelet packet tree with decomposition depth J , the information cost of the node is , where is j number of decomposition layers, n is frequency index, and k is time position. Dynamic Programming Algorithm for Best Base Selection:

1) The information cost of the nodes at the bottom of the calculation tree:

$$\lambda_{J,n,k} = E(w_{J,n,k}) \tag{8}$$

2) Recursively calculate the optimal cost of each node from the bottom up:

$$\lambda_{j,n,k} = \min\{E(w_{j,n,k}), \lambda_{j+1,2n,k} + \lambda_{j+1,2n+1,k}\} \tag{9}$$

The decision function is:

$$D_{j,n,k} = \begin{cases} 1, & \text{if } E(w_{j,n,k}) \le \lambda_{j+1,2n,k} + \lambda_{j+1,2n+1,k} \\ 0, & \text{otherwise} \end{cases} \tag{10}$$

Based on the above optimal basis selection criteria, the main steps of the adaptive wavelet packet decomposition algorithm are as follows:

(1) Initialization: The input signal is decomposed into the first layer by decomposing the complete wavelet packet to obtain the coefficient:

$$w_{j,n,k} = \langle x, \psi_{j,n,k} \rangle \tag{11}$$

where the wavelet packet basis function satisfies orthogonality:

$$\langle \psi_{j,n,k}, \psi_{j',n',k'} \rangle = \delta_{j,j'} \delta_{n,n'} \delta_{k,k'} \tag{12}$$

(2) Calculate the information cost: calculate the information cost for each node $\lambda j, n, k$.

(3) Best base search: The dynamic programming algorithm is used to determine the best base, and its mathematical expression is:

$$B = \arg\min_B \sum_{(j,n,k)\in B} \lambda_{j,n,k} \tag{13}$$

Completeness conditions are met:

$$\sum_{(j,n,k)\in B} |\langle x, \psi_{j,n,k} \rangle|^2 = \| x \|^2 \tag{14}$$

(4) Coefficient threshold treatment: soft threshold or hard threshold treatment for the optimal basis coefficient:

$$\hat{w}_{j,n,k} = \begin{cases} \text{sign}(w_{j,n,k})(|w_{j,n,k}| - \tau), & |w_{j,n,k}| > \tau \\ 0, & \text{otherwise} \end{cases} \tag{15}$$

where the threshold τ can be determined by various criteria, such as the universal threshold:

$$\tau = \sigma\sqrt{2\log N} \tag{16}$$

σ is the noise standard deviation, and N is the signal length.

3.2. Wave Atom transform

The core of the WaveAtom transform is the decomposition of the signal through the wave atomic basis function. Wave atoms are a class of basis functions with localized properties that are capable of providing high resolution in both the time and frequency domains, similar to wavelet transforms but optimized for sparsity. Features include:

The signal is decomposed by the basis function of different scales, similar to the multi-resolution property of wavelets, but the basis function of the wave atom may have a more compact support interval. It is suitable for capturing edge and texture information in images, similar to curvelet transformations, but with less computational complexity. In addition, the noise and signal are separated by threshold processing of high-frequency coefficients, similar to the wavelet threshold denoising method.

The Wave Atom basis function is a family of functions with specific time-frequency localization properties. Its basic form can be expressed as:

$$\varphi_\mu(x) = \varphi_{j,m,n}(x) = 2^j \varphi(2^j x - n) \cdot e^{i 2^j m \cdot x} \tag{17}$$

The basis function satisfies the following support conditions:

Time domain support:

$$\text{supp } \varphi_\mu \subset \{x : |x - 2^{-j} n| \le C_1 \cdot 2^{-j}\} \tag{18}$$

Frequency domain support:

$$\text{supp } \hat{\varphi}_\mu \subset \{\xi : |\xi - 2^j m| \le C_2 \cdot 2^j\} \tag{19}$$

C_1, C_2 are normal numbers. The following orthogonality conditions need to be met for the basis function family:

$$\langle \varphi_\mu, \varphi_{\mu'} \rangle = \delta_{\mu,\mu'} \tag{20}$$

For 2D signal $f(x) \in L^2(\mathbb{R}^2)$, its Wave Atom transform is defined as:

$$W_f(\mu) = \langle f, \varphi_\mu \rangle = \int_{\mathbb{R}^2} f(x) \overline{\varphi_\mu(x)} dx \tag{21}$$

The inverse transformation can be expressed as:

$$f(x) = \sum_\mu W_f(\mu) \varphi_\mu(x) \tag{22}$$

The summation range includes all scale, direction, and positional parameters.

Wave Atom has a unique parabolic scale relationship in the time-frequency plane:

$$|\Delta x|^2 \approx |\Delta \xi|^{-1} \tag{23}$$

|Δx| denotes the spatial localization range, |Δξ| Indicates the frequency localization range.

The energy distribution function can be expressed as:

$$E_\mu(x,\xi) = |\varphi_\mu(x)|^2 \cdot |\hat{\varphi}_\mu(\xi)|^2 \tag{24}$$

Satisfy:

$$\int_{\mathbb{R}^2}\int_{\mathbb{R}^2} E_\mu(x,\xi)dxd\xi = 1 \tag{25}$$

In the discrete domain, the Wave Atom transform can be achieved with the following steps:

(1) Fast Fourier transform:

$$\hat{f}[k] = \sum_{n=0}^{N-1} f[n]e^{-2\pi ikn/N} \tag{26}$$

(2) Frequency domain allocation:

$$\hat{\varphi}_{j,m}(\xi) = g(2^{-j}\xi - m) \tag{27}$$

(3) Frequency domain modulation:

$$\hat{W}_f(j,m,n) = \hat{f}(\xi)\cdot\hat{\varphi}_{j,m}(\xi) \tag{28}$$

(4) Inverse Fourier transform:

$$W_f(j,m,n) = \sum_{k=0}^{N-1}\hat{W}_f(j,m,k)e^{2\pi ikn/N} \tag{29}$$

3.3. Curvelet transforms

As an important breakthrough in the second-generation wavelet theory, the core idea of the Curvelet transform stems from the mathematical modeling of the geometric characteristics of high-dimensional signals. In the field of two-dimensional signal processing, the traditional wavelet transform is limited by the essential defects of isotropic basis functions, and shows obvious limitations in processing images with directional sensitivity and curvilinear singularity. The Curvelet transform theory proposed by Candès and Donoho successfully achieves the optimal sparse representation of the curvilinear singularity in the image by introducing a direction-sensitive multi-scale analysis framework.

The mathematical foundation of the transformation is based on the intersection of harmonic analysis and differential geometry, and its core innovation is reflected in three key dimensions; The anisotropic scaling mechanism of the parabolic scale, the direction-sensitive frequency space division and the tight support characteristics of the space-frequency localization.

This unique multi-resolution structure enables Curvelet to approximate the two-dimensional piecewise smooth function with smooth boundary at a near-optimal convergence rate, which provides a new mathematical tool for solving the problem of geometric feature extraction in image processing.

The mathematical definition of the Curvelet basis function is based on strict affine transform group theory, and its parameterization process consists of three key operations:

$$\varphi_{j,l,k}(x) = 2^{\frac{3j}{4}}\varphi\left(D_2^j R_{\theta_l}(x - x_{j,l,k})\right) \tag{30}$$

In this way, the basis function presents an elongated elliptic shape in the space, and the direction of the major axis changes with θ_l, and the length of the minor axis is proportional to the square of the length of the major axis, which perfectly fits the geometric characteristics of the curve features.

4. Result and Analysis

4.1. Impact of Damage Severity.

damage located in elements numbered 32740 and 32741, comprising a total of two damaged elements. This section evaluates the performance and clarity of three signal processing methods—Wave Atom Transform, Wavelet Packet Transform, and Curvelet Transform—on damage location identification. Five different damage severity conditions were designed, with damage gradients set at 50%, 30%, 10%, 5%, and 1%.

Under the first condition, with 50% damage severity, the Z-direction displacement data is used to apply Wave Atom Transform, Wavelet Packet Transform, and Curvelet Transform. Figure 3 displays the resulting coefficient distribution from the transformations. From the figure, it is evident that all three methods perform reasonably well in identifying the damage location. However, as the damage level decreases, the clarity of the damage location in the Wave Atom and Curvelet transforms diminishes. The Wave Atom and Curvelet transformations are more effective at higher damage levels, while lower damage levels result in less defined damage localization. In contrast, the Wavelet Packet Transform accurately and clearly identifies the damage location, although the transient model's excitation points are also identified as high-frequency components, leading to an "over-interpretation" phenomenon.

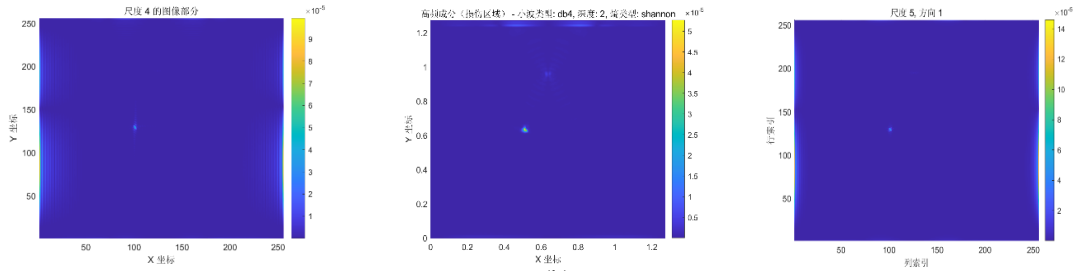

(a) (b) (c)

Figure 3. The Z-direction displacement under the transient damage severity condition 1: (a) Wave atom transform coefficient diagram; (b) Wavelet packet transform coefficient diagram; (c) Curvelet transform coefficient distribution diagram

In case 2 (damage degree of 30%), based on the Z-direction displacement data, the model is transformed by Wave atom transform, wavelet packet transform and curvelet transform. Figure 4 shows the coefficient distribution after transformation.

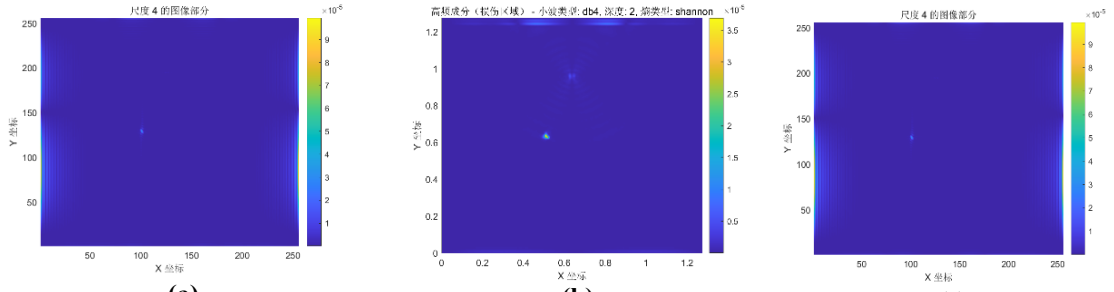

(a) **(b)** **(c)**

Figure 4. The Z-direction displacement under the transient damage severity condition 2: (a) Wave atom transform coefficient diagram; (b) Wavelet packet transform coefficient diagram; (c) Curvelet transform coefficient distribution diagram

In case 3 (damage degree of 10%), based on the Z-direction displacement data, the model is transformed by Wave atom transform, wavelet packet transform and curvelet transform. Figure 5 shows the coefficient distribution after transformation.

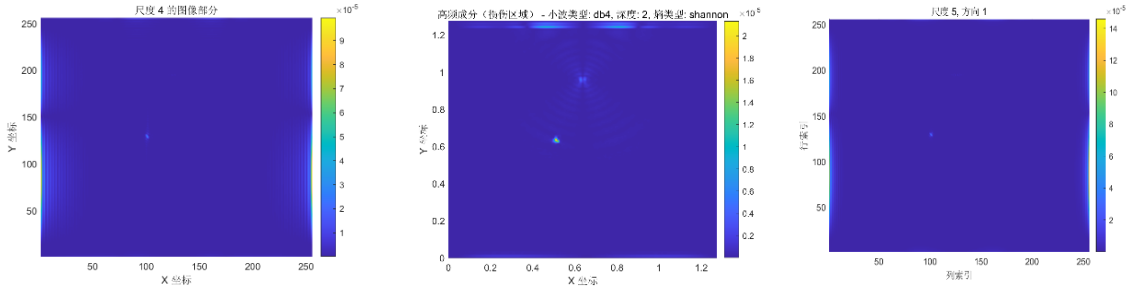

(a) (b) (c)

Figure 5. The Z-direction displacement under the transient damage severity condition 3: (a) Wave atom transform coefficient diagram; (b) Wavelet packet transform coefficient diagram; (c) Curvelet transform coefficient distribution diagram

In case 4 (damage degree of 5%), based on the Z-direction displacement data, the Wave atom transform, wavelet packet transform and curvelet transform were performed on the model. Figure 6 shows the coefficient distribution after transformation.

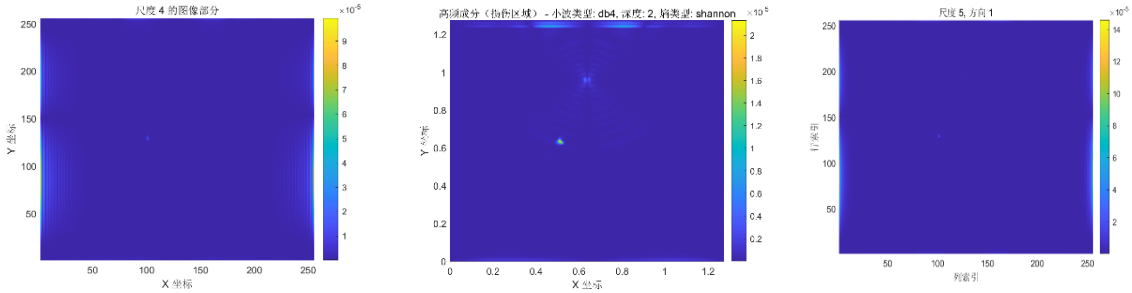

(a) (b) (c)

Figure 6. The Z-direction displacement under the transient damage severity condition 4: (a) Wave atom transform coefficient diagram; (b) Wavelet packet transform coefficient diagram; (c) Curvelet transform coefficient distribution diagram

In case 5 (damage degree of 1%), based on the Z direction displacement data, the Wave atom transform, wavelet packet transform and curvelet transform were performed on the model. Figure 7 shows the coefficient distribution after transformation.

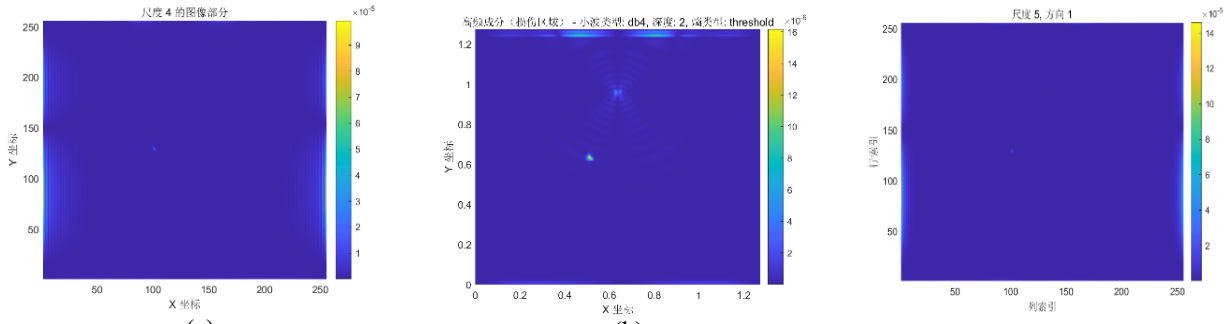

(a) (b) (c)

Figure 7. The Z-direction displacement under the transient damage severity condition 5: (a) Wave atom transform coefficient diagram; (b) Wavelet packet transform coefficient diagram; (c) Curvelet transform coefficient distribution diagram

In the recognition and analysis of transient damage sheet models from case 1 to case 5, the Wave atom transform and curvelet transform can accurately identify the precise location of the damage, and gradually blur with the reduction of the damage degree, which is conducive to the quantitative evaluation of the damage. In the analysis of the transient model, due to its limited spatial localization ability, it is easy to parse the excitation action point as a high-frequency feature, forming an "over-analysis" phenomenon, but it has little impact on the accuracy of damage location identification. From the perspective of identifying the degree of damage, the Wave atom transform has the best effect, followed by the curvelet transform, and the wavelet packet is relatively poor.

4.2. Effect of Extent of Injury

Five kinds of working conditions with different damage ranges of 50% damage degree are set up.

The damage range of condition 1 is 0.01m×0.01m, and the damage units are: 32740, 32741, 32995, 32996

The damage range of condition 2 is 0.02m×0.02m, and the damage units are: 32484-32487, 32739-32742, 32994-32997, 33249-33252

The damage range of condition 3 is 0.03m×0.03m, and the damage units are: 32227-32232, 32482-32487, 32737-32742, 32992-32997, 33247-33252, 33502-33507

The damage range of condition 4 is 0.04m×0.04m, and the damage units are: 31971-31978, 32226-32233, 32481-32488, 32736-32743, 32991-32998, 33246-33253, 33501-33508, 33756-33763

The damage range of condition 5 is 0.05m×0.05m, and the damage units are: 31715-31724, 31970-31979, 32225-32234, 32480-32489, 32735-32744, 32990-32999, 33245-33254, 33500-33509, 33755-33764, 34010-34019

The Wave atom transform, wavelet packet transform and curvelet transform are performed on the transient damage range case 1 model, and Figure 8 shows the distribution of the Z-direction displacement Wave atom transform, wavelet packet transform and curvelet transformation coefficients under the transient damage range case.

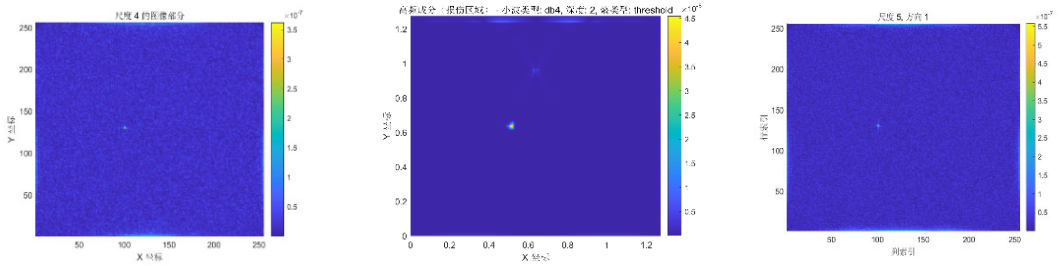

(a) (b) (c)

Figure 8. Z-direction displacement under the transient damage range operating condition 1: (a) Wave atom transform coefficient diagram; (b) Wavelet packet transform coefficient diagram; (c) Curvelet transform coefficient distribution diagram

The Wave atom transform, wavelet packet transform and curvelet transform are performed on the transient damage range case 2 model, and Fig. 9 shows the distribution of the Z-direction displacement Wave atom transform, wavelet packet transform and curvelet transform coefficients under the transient damage range case 2.

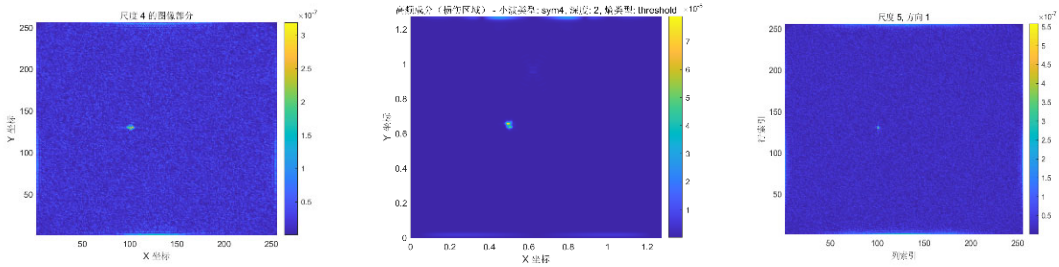

(a) **(b)** **(c)**

Figure 9. Z-direction displacement under the transient damage range operating condition 2: (a) Wave atom transform coefficient diagram; (b) Wavelet packet transform coefficient diagram; (c) Curvelet transform coefficient distribution diagram

The Wave atom transform, wavelet packet transform and curvelet transform are performed on the three models of the transient damage range, and Figure 10 shows the distribution of the coefficient distribution of the Z-direction displacement Wave atom transform, wavelet packet transform and curvelet transform under the three transient damage range cases.

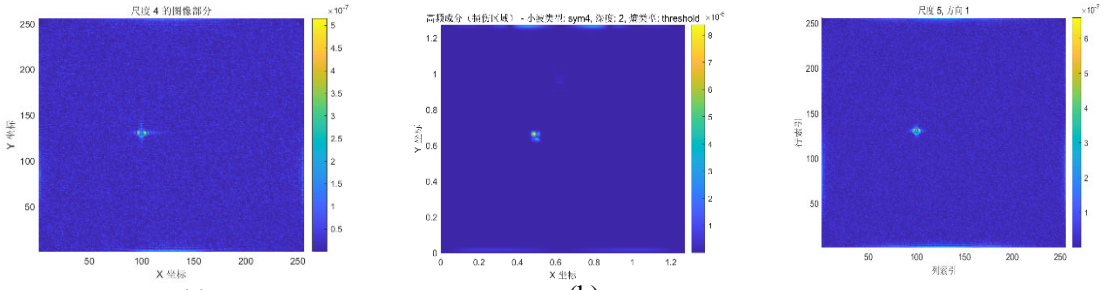

(a) (b) (c)

Figure 10. Z-direction displacement under the transient damage range operating condition 3: (a) Wave atom transform coefficient diagram; (b) Wavelet packet transform coefficient diagram; (c) Curvelet transform coefficient distribution diagram

The Wave atom transform, wavelet packet transform and curvelet transform are performed on the four models of the transient damage range, and Figure 11 shows the distribution of the coefficient distribution of the Z-direction displacement Wave atom transform, wavelet packet transform and curvelet transform under the four transient damage range cases.

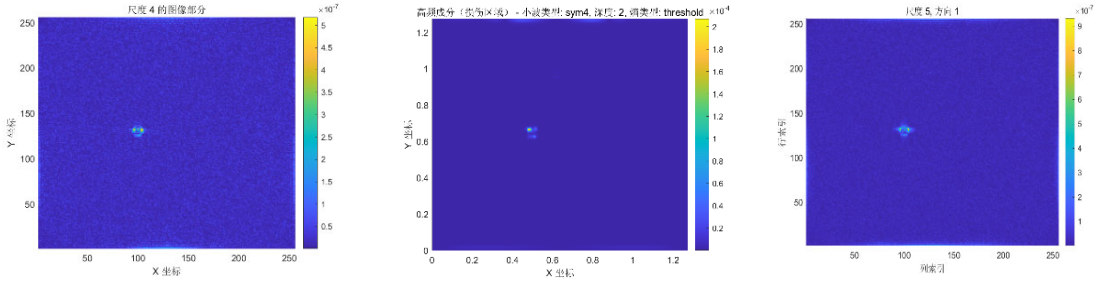

(a) (b) (c)

Figure 11. Z-direction displacement under the transient damage range operating condition 4: (a) Wave atom transform coefficient diagram; (b) Wavelet packet transform coefficient diagram; (c) Curvelet transform coefficient distribution diagram

Figure 12 shows the distribution of the coefficient distribution of Z-direction displacement Wave atom transform, wavelet packet transform and curvelet transform under the fifth transient damage range case.

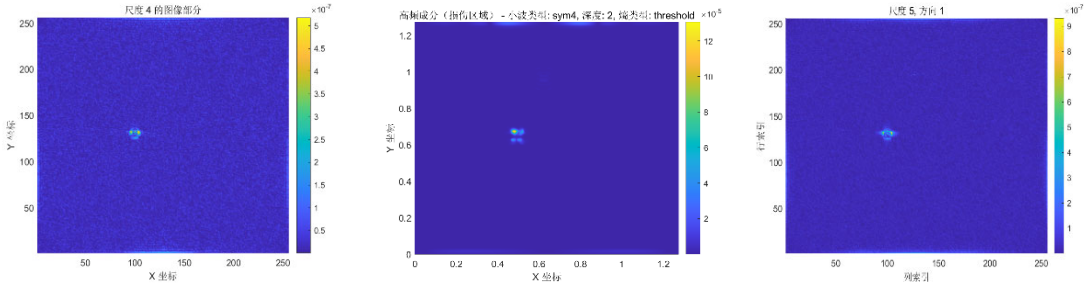

(a) (b) (c)

Figure 12. Z-direction displacement under the transient damage range operating condition 5: (a) Wave atom transform coefficient diagram; (b) Wavelet packet transform coefficient diagram; (c) Curvelet transform coefficient distribution diagram

In the first three working conditions, the wavelet packet transformation expansion can accurately locate the damage area, clearly depict the damage boundary and internal details of the damage, and maintain a high signal-to-noise ratio. In the fourth case, the recognition ability of the wavelet packet transform is attenuated. Although the wavelet packet transform can still identify the general contour of the damage, the ability to depict the internal details of the damage is obviously insufficient, and it is difficult to take into account the representation of both macro contour and micro details. However, compared with the static damage model data, the Wave Atom transform and Curvelet transform have significantly lower pseudofeatures under all working conditions.

4.3. Identification of boundary damages

Four kinds of boundary damage conditions are set, and the damage degree is 50%. The first boundary damage case is the vertical continuous element strip damage, and the boundary damage case 2 is the transverse continuous element strip damage. The third boundary damage case is oblique downward continuous element strip damage. The fourth boundary damage case is the oblique continuous element strip damage. The adaptability of wavelet packet transform to

boundary damage is studied.

The plate damage units of boundary damage case 1 are: 31633, 31888, 32143, 32398, 32653, 32908, 33163, 33418, 33673, 33928.

The thin plate damage units of boundary damage case 2 are: 31633, 31634, 31635, 31636, 31637, 31638, 31639, 31640, 31641, 31642.

The plate damage elements of boundary damage case 3 are: 31633, 31889, 32145, 32401, 32657, 32913, 33169, 33425, 33681, 33937.

The plate damage units of boundary damage case 4 are: 31633, 31887, 32141, 32395, 32649, 32903, 33157, 33411, 33665, 33919.

The Wave Atom transform, wavelet packet transform and Curvelet transform are performed on the boundary damage case 1 model. Figure 13 shows the distribution of the (a) Wave Atom transform, (b) wavelet packet transform, and (c) Curvelet transform coefficients of the Z-direction deflection under the boundary damage case.

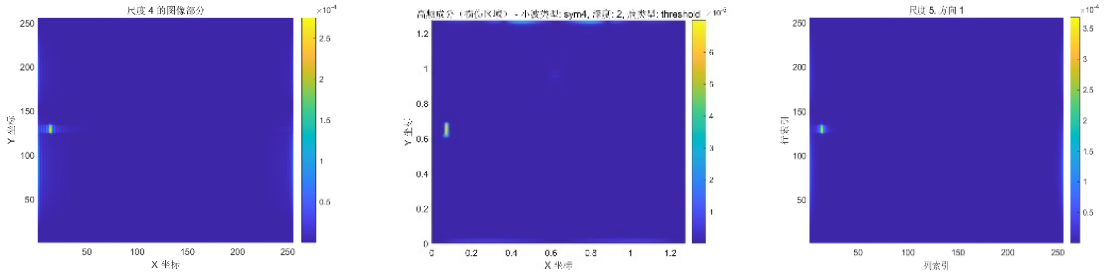

(a) (b) (c)

Figure 13. Z-direction displacement under the transient boundary damage condition 1: (a) Wave atom transform coefficient diagram; (b) Wavelet packet transform coefficient diagram; (c) Curvelet transform coefficient distribution diagram

The Wave Atom transform, wavelet packet transform and Curvelet transform are performed on the boundary damage case 2 model. Figure 14 shows the distribution of the coefficient distribution of the (a) Wave Atom transform, (b) wavelet packet transform, and (c) Curvelet transform coefficients of the Z-direction deflection under boundary damage case 2.

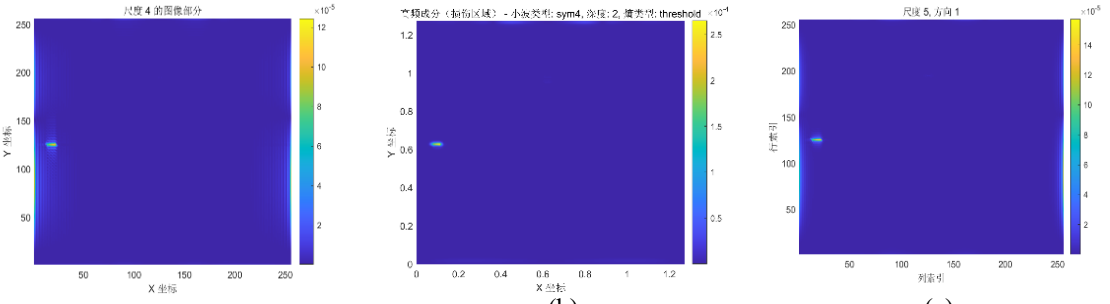

(a) (b) (c)

Figure 14. Z-direction displacement under the transient boundary damage condition 2: (a) Wave atom transform coefficient diagram; (b) Wavelet packet transform coefficient diagram; (c) Curvelet transform coefficient distribution diagram

The Wave Atom transform, wavelet packet transform and Curvelet transform were performed on the boundary damage case three models. Figure 4.15 shows the distribution of the coefficients of the Z-direction deflection (a) Wave Atom transform, (b) wavelet packet transform, and (c) Curvelet transformation under the three boundary damage cases.

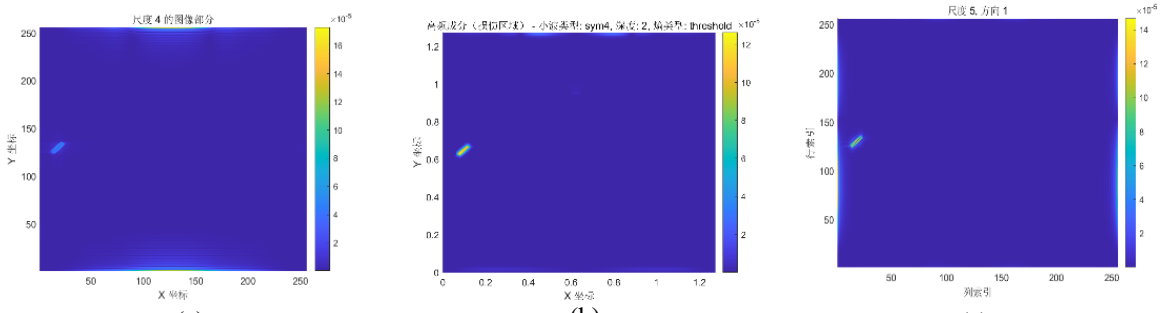

(a) (b) (c)

Figure 15. Z-direction displacement under the transient boundary damage condition 3: (a) Wave atom transform coefficient diagram; (b) Wavelet packet transform coefficient diagram; (c) Curvelet transform coefficient distribution diagram

The Wave Atom transform, wavelet packet transform and Curvelet transform were performed on the boundary damage case four models. Fig. 16 shows the distribution of the coefficients of the Z-direction deflection (a) Wave Atom transform, (b) wavelet packet transform and (c) Curvelet transform under the boundary damage case.

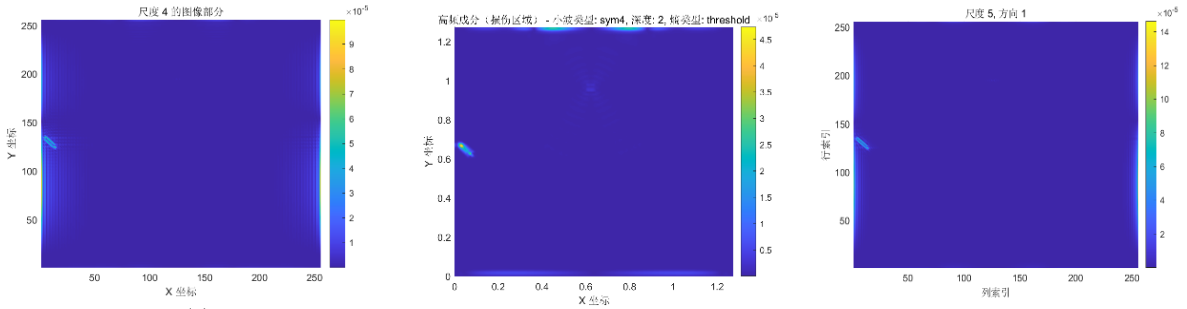

(a) (b) (c)

Figure 16. Z-direction displacement under the transient boundary damage condition 4: (a) Wave atom transform coefficient diagram; (b) Wavelet packet transform coefficient diagram; (c) Curvelet transform coefficient distribution diagram

The three transformation methods can identify the location of the damage well, and the difference is weak.

5. Conclusion

In this chapter, the Wave Atom transform, wavelet packet transform and Curvelet transform signal processing methods are used to evaluate their performance and adaptability in the transient damage model.

We simulate the dynamic response under external excitation through transient analysis to study the dynamic effect of damage on the thin plate structure. By comparing different damage degrees (50%, 30%, 10%, 5%, 1%) and different damage ranges, the damage identification effect of the three transformation methods under dynamic response was evaluated. In the transient analysis, the Wave Atom transform can effectively capture the high-frequency response, and has obvious coefficient peaks for more severe injuries (such as 30% and 50%), which can accurately locate the damage area. However, in the case of mild damage (e.g., 10% and 5%), the recognition effect of the Wave Atom transform is poor, and the coefficient of the damage location is not obvious enough, which is difficult to accurately locate. The wavelet packet transform shows high positioning accuracy in the transient response, and can clearly locate the damage even when the damage is light. Due to the limited spatial localization ability of wavelet packet transform, it is easy to resolve the high-frequency components of external excitation into damage characteristics in transient analysis, resulting in the phenomenon of "over-resolution". Similar to the Wave Atom transform, the curvelet transform has poor performance under mild damage and is difficult to effectively extract damage information.

References

[1] Xiang Dong. Wavelet Analysis of Weak Signal Feature Extraction Under Strong Noise Background [D]. Wuhan University, 2006.

[2] Rytter A. Vibration based inspection of civil engineering structures Ph. D[J]. Aalborg University, Aalborg, Denmark, 1993.

[3] Sining Huang,Ran Zheng,Xiao Sun,Tiantian Qiao,Feiyu Zhang.Efficient structural damage detection via the lω regularization and randomized extended Kaczmarz algorithm [J]. Structural Health Monitoring,2024,23(5):3211-3226.

[4] Liu W ,Wang S ,Yin Z , et al.Structural damage detection of switch rails using deep learning [J]. NDT and E International, 2024, 147103205-103205.

[5] Makiabadi H M ,Maheri R M ,Sarcheshmehpour M .Damage Detection of Span Bridge Structures Under Moving Loads Using the Hybrid Enhanced SOS-SA Algorithm[J].Iranian Journal of Science and Technology, Transactions of Civil Engineering,2024,(prepublish):1-17.

[6] Yuan P P ,Zhao J Z ,Cheng L X , et al.Research on damage identification of jacket structure under wind and wave loads based on variational mode decomposition and chirplet transform[J].Journal of Vibration and Control,2025,31(5-6):1005-1021.

[7] Yang Haijun, Ma Lei, Xu Yongzhi, et al. Structural damage recognition method based on improved modal strain energy and DBO-BP neural network [J]. Mechanics Quarterly, 2025, 46(01): 118-129.DOI:10.15959/j.cnki.0254-0053.2025.01.011.

[8] Barbosh M ,Sadhu A .Wavelet packet transformation-based improved acoustic emission method for structural damage identification [J].Smart Materials and Structures, 2025, 34(1): 015036-015036.

[9] Yao Xiaojun, Sun Shoupeng, Wang Qiang, et al. Research on structural damage identification method combining variational modal decomposition and time series model[J].Vibration & Shock, 2025, 44(05): 131-139+217. DOI:10.13465/j.cnki.jvs.2025.05.015.

[10] Yanfang H ,Weibing H ,Xin W , et al.Damage Identification of Ancient Timber Structure Based on Autocorrelation Function [J]. Advances in Civil Engineering,2021,2021

[11] Moharana S .Investigation of a Continuum Shear Lag Model as an Indicator for the Damage Detection in Piezo-Elasto Dynamic Structure [J]. Journal of Vibration Engineering & Technologies, 2021, 9(7):1-14.

[12] Lu Y ,Tang L ,Liu Z , et al.Unsupervised quantitative structural damage identification method based on BiLSTM networks and probability distribution model [J]. Journal of Sound and Vibration, 2024, 590118597-118597.

[13] Hu Qiang, Cai Xiaoli, Li Cui, et al. Earthquake Engineering and Engineering Vibration,2024,44(03):61-72.DOI:10.13197/j.eeed.2024.0306.